UTAP-408
Preprint typeset using LaTeX style emulateapj v. 25/04/01

SYSTEMATIC EFFECTS ON TANGENTIAL AND RADIAL ARC STATISTICS: THE FINITE SOURCE SIZE AND ELLIPTICITIES OF THE LENS AND SOURCE

MASAMUNE OGURI
Department of Physics, School of Science, University of Tokyo, Tokyo 113-0033, Japan.
oguri@utap.phys.s.u-tokyo.ac.jp
UTAP-408

ABSTRACT

It has been recognized that the arc statistics of gravitational lensing is a useful probe of the density profile of clusters of galaxies. We examine several systematic effects which are important in predicting the number of arcs, with particular attention to the difference between tangential and radial arcs. First we derive an analytic expression of the cross section for radial arcs taking account of the source size and find that the moderate source size enhances the cross section for radial arcs while larger source size ($\gtrsim 1''$ in our example) suppresses the number of radial arcs. On the other hand, tangential arcs are much less sensitive to the source size. Next we numerically calculate the cross section for arcs considering the lens and source ellipticities. We find that the numbers of both tangential and radial arcs are highly enhanced by both ellipticities, by one or two orders of magnitude. The number ratio of radial to tangential arcs is, however, not so affected if the threshold axis ratio of arcs is large ($\gtrsim 7$). The number ratio therefore still remains good statistics which probe the density profile of the lens objects, if the source size effect is correctly taken into account.

Subject headings: cosmology: theory — dark matter — galaxies: clusters: general — gravitational lensing

1. INTRODUCTION

Clusters of galaxies distort the images of background galaxies due to the gravitational lensing effect. The statistics of such lensed arcs have been recognized as a powerful probe of the density profile of lens clusters (Wu & Hammer 1993; Miralda-Escudé 1993a; Bartelmann 1996; Hattori, Watanabe, & Yamashita 1997; Williams, Navarro, & Bartelmann 1999; Molikawa et al. 1999; Meneghetti et al. 2001). In particular, combined statistics of tangential and radial arcs are useful in determining the density profile of clusters (Molikawa & Hattori 2001; Oguri, Taruya, & Suto 2001). A knowledge of the density profile is important because of recent indications that the cold dark matter scenario predicts a cuspy profile (e.g., Navarro, Frenk, & White 1996, 1997) while observations seem to prefer the existence of flat density cores (e.g., Tyson, Kochanski, & Dell'Antonio 1998).

Most of the previous analytic work assume the infinitesimally small size of source galaxies. As pointed out by Molikawa & Hattori (2001) and Oguri et al. (2001), however, the cross section for radial arcs may be severely affected by the finite source size. Moreover, finite size sources can produce the fold image, thus the cross section may be somewhat different from the one obtained by assuming the infinitesimal source size. Therefore, we analytically calculate the cross section for radial arcs including the source size effect. We also derive the cross section using Monte Carlo method and compare this with theoretical predictions.

Another systematic effect is due to the asymmetry in the mass distribution of the lens cluster (Bartelmann, Steinmetz, & Weiss 1995; Bartelmann 1995; Flores, Maller, & Primack 2000; Meneghetti et al. 2000; Meneghetti, Bartelmann, & Moscardini 2002). Bartelmann et al. (1995) claimed that the numerically modeled clusters produce long arcs about two orders of magnitude more frequently than spherically symmetric cluster models. Therefore, we also study the effects of asymmetries of lens objects. Especially we concentrate on the difference of asymmetry effects between tangential and radial arcs. As for the source ellipticity, Keeton (2001) analytically calculated the cross section including the source ellipticity and found that the effect of the source ellipticity is small compared with the effect of different density profiles. Nevertheless we also examine the effect of the source ellipticity in order to check the theoretical predictions and to see the effect of different threshold axis ratios of arcs.

This paper is organized as follows. In §2, we analytically derive the cross section for radial arcs including the finite source size. Section 3 describes the simulation method, and §4 presents the cross section derived by numerical simulations. The validity of our selection criterion for tangential and radial arcs is discussed in §5. Finally, we summarize the results in §6. Throughout this paper, we assume the lambda-dominated cosmology $(\Omega_0, \lambda_0) = (0.3, 0.7)$. The Hubble constant in units of $100\mathrm{km\,s^{-1}Mpc^{-1}}$ is denoted by h.

2. CROSS SECTION FOR RADIAL ARCS WITH FINITE SOURCE SIZE

The previous analytic work often assumed the infinitesimal size of source galaxies. On the other hand, it has been pointed out that the finite source size affects the cross section particularly for radial arcs (Molikawa & Hattori 2001; Oguri et al. 2001). Moreover, sources with a finite size have a possibility to produce the fold image which is formed by merging two images near the radial critical curve, even in the case of the spherical symmetric lens. Therefore, the cross section for radial arcs including the finite source size effect may be somewhat different from the one calculated by neglecting the source size. In this section, we derive an analytic expression of the cross section for radial arcs taking account of the finite size of source galaxies assuming spherical lenses.

The image position $\vec{\xi}$ in the lens plane corresponding to the source at $\vec{\eta}$ in the source plane is determined by the lens equation (e.g., Schneider, Ehlers, & Falco 1992):

$$y = x - \alpha(x), \tag{1}$$

where $x = |\vec{x}| = |\vec{\xi}|/\xi_0$, $y = |\vec{y}| = |\vec{\eta}|D_{\rm OL}/(\xi_0 D_{\rm OS})$, and $D_{\rm OL}$ and $D_{\rm OS}$ denote the angular diameter distances from the observer to

the lens and the source planes, respectively. The normalization length ξ_0 can be arbitrary. The deflection angle $\alpha(x)$ is related to the mass distribution of the lens object. In the case of spherical lenses, a source at x is stretched by the factor $\mu_t(x) \equiv (y/x)^{-1}$ along the tangential direction and $\mu_r(x) \equiv (dy/dx)^{-1}$ along the radial direction. Then for the infinitesimal source, the cross sections for tangential and radial arcs are simply given by the areas in the source plane in which the inequalities:

$$\text{Tangential arc}: \quad T(x) \equiv \left| \frac{\mu_t(x)}{\mu_r(x)} \right| \geq \epsilon_{\rm th} \tag{2}$$

$$\text{Radial arc}: \quad R(x) \equiv \left| \frac{\mu_r(x)}{\mu_t(x)} \right| \geq \epsilon_{\rm th} \tag{3}$$

are satisfied. For the threshold axis ratio, e.g., Oguri et al. (2001) adopted $\epsilon_{\rm th} = 4$. Since the assumption that the source size is sufficiently small seems to be valid for usual tangential arcs (see Hattori et al. 1997), in this paper we use equation (2) to predict the cross section for tangential arcs.

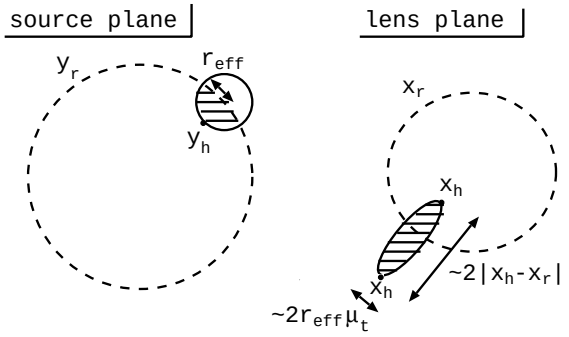

FIG. 1.— A schematic diagram of the lens mapping in forming a fold image. The radial critical line (with radius x_r) and radial caustic (with radius y_r) are shown by dashed lines. If the source cross the radial caustic, only a part of the source inside the radial caustic (denoted by the shading) is mapped into near the radial critical line. Then $r_{\rm eff}$ (eq. [7]) means the effective radius of the shaded part of the source. The radius of the point in the source which is nearest from the center of the lens is denoted by y_h, and either radius of corresponding two points in the lens plane is x_h. In this situation, the criterion for radial arcs is well approximated by equation (5).

Consider the cross section for radial arcs when the source has the finite size. First we consider the fold images. These images are produced only when sources cross the radial caustic:

$$y_r - r_S \equiv y_- \leq y \leq y_+ \equiv y_r + r_S, \tag{4}$$

where y_r is the radius of the radial caustic and r_S is the dimensionless source radius. In this situation, we approximate the criterion for radial arcs as (see Figure 1)

$$R_f(x_h) \equiv \frac{|x_h - x_r|}{\mu_t(x_r) r_{\rm eff}} \geq \epsilon_{\rm th}, \tag{5}$$

where x_r is the radius of the radial critical line and x_h denotes two farthest points from the radial critical line. The latter is related to the center of the source y as

$$y = y_h - r_S, \tag{6}$$

with $y_h = |y(x_h)|$ being the radius corresponding to x_h. The effective radius of the source $r_{\rm eff}$ in equation (5) is defined by

$$r_{\rm eff} \equiv \begin{cases} \sqrt{r_S^2 - (y_r + r_S - y_h)^2} & (y_r < y_h - r_S), \\ r_S & (y_r \geq y_h - r_S). \end{cases} \tag{7}$$

We calculate the cross section as the area in the source plane in which the condition (5) is satisfied at both sides of the radial critical line in the image plane, that is, the area in which the following condition is satisfied:

$$y < y_f \equiv \min(y_{h+} - r_S, y_{h-} - r_S), \tag{8}$$

where $y_{h\pm} = |y(x_{h\pm})|$ are two radii corresponding to solutions of the equation $R_f(x_{h\pm}) = \epsilon_{\rm th}$ at both sides of the radial critical line.

Next consider images which do not touch the radial critical line. These images are possible only for

$$y < y_-. \tag{9}$$

Except for this condition, the cross section can be calculated similarly as the one with infinitesimal source size, and is explicitly expressed as

$$y_r > y > y_u \equiv \min(y_{u+}, y_{u-}), \tag{10}$$

where $y_{u\pm} = |y(x_{u\pm})|$ are two radii corresponding to solutions of the equation $R(x_{u\pm}) = \epsilon_{\rm th}$ at both sides of the radial critical line.

Combining equations (4), (8), (9), and (10), the cross section for radial arcs $\sigma_{\rm rad}$ is written as

$$\sigma_{\rm rad} = \left(\frac{\xi_0 D_{\rm OS}}{D_{\rm OL}} \right)^2 S(\min(y_+, y_f), \max(y_-, y_u)), \tag{11}$$

where $S(a,b)$ is defined by

$$S(a,b) \equiv \begin{cases} \pi(a^2 - b^2) & (a > b), \\ 0 & (a < b). \end{cases} \tag{12}$$

The radii y_+, y_-, y_f, and y_u are defined by equations (4), (4), (8), and (10), respectively.

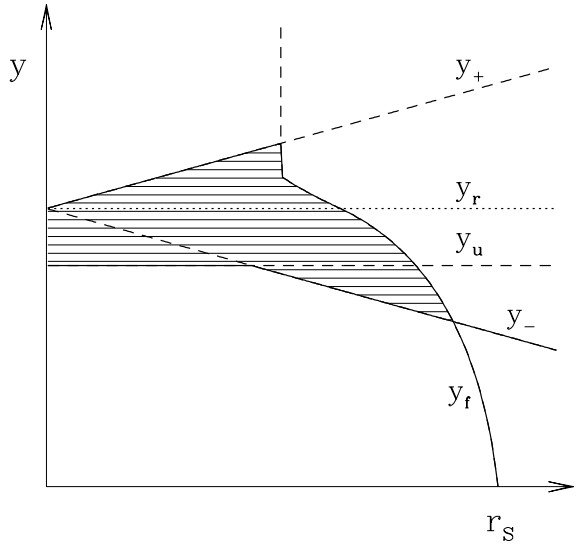

FIG. 2.— Dependence of radii defined in order to calculate the cross section for radial arcs, y_+ (eq. [4]), y_- (eq. [4]), y_f (eq. [8]), and y_u (eq. [10]), on the source radius r_S. The radius of the radial caustic y_r is also shown for reference. The definition of each radius is given in §2. The shading indicates the region where radial arcs are formed.

Figure 2 shows the dependence of each radius defined in the above on the source radius r_S. This figure indicates that the moderate amount of source size *enhances* the cross section, while the larger source size significantly decreases the cross section.

3. SIMULATION METHOD

In this section, we briefly describe the mapping and detecting algorithm of arcs. Most of our method described in §3.2 and §3.3 follows the work by Miralda-Escudé (1993b) and Bartelmann & Weiss (1994).

3.1. *Lens Model*

For density profiles of clusters, we adopt the generalization of those proposed by Navarro et al. (1996, 1997), the generalized NFW profile (Jing & Suto 2000):

$$\rho(r) = \frac{\rho_{\rm crit}\delta_{\rm c}}{\left(r/r_{\rm s}\right)^{\alpha}\left(1+r/r_{\rm s}\right)^{3-\alpha}}. \tag{13}$$

For this profile, we choose the normalization of the lens equation as $\xi_0 = r_{\rm s}$. The concentration parameter $c_{\rm vir} = r_{\rm vir}/r_{\rm s}$, where $r_{\rm vir}$ is the virial radius of dark halo, depends on the halo mass M and the redshift $z_{\rm L}$. We calculate $c_{\rm vir}$ using the fitting form derived by Bullock et al. (2001):

$$c_{\rm vir} = \frac{8}{1+z_{\rm L}}\left(\frac{M}{10^{14}h^{-1}M_{\odot}}\right)^{-0.13}, \tag{14}$$

for $\alpha = 1$, and we generalize it to $\alpha \neq 1$ by multiplying $(2-\alpha)$ (see Keeton & Madau 2001).

Ellipticities of the lens and source are included as follows. For the lens ellipticity, we simply substitute u for x in the axially symmetric lens potential $\psi(x)$:

$$u^2 = (1-e_{\rm L})x_1^2 + \frac{x_2^2}{1-e_{\rm L}}, \tag{15}$$

where $\vec{x} = (x_1, x_2)$. With this substitution, the ellipticity is $e_{\rm L} = 1-b/a$, where a and b are the semi-major and semi-minor axes. Then the deflection angle α is obtained by

$$\alpha(x_1) = \frac{(1-e_{\rm L})x_1}{u}\alpha(u), \tag{16}$$

$$\alpha(x_2) = \frac{x_2}{(1-e_{\rm L})u}\alpha(u), \tag{17}$$

where $\alpha(u)$ is the deflection angle for the axially symmetric lens. Note that this elliptical model is same as the one adopted by Meneghetti et al. (2002; see also Golse & Kneib 2002). The source ellipticity is included in the detection of images (eq. [18]).

3.2. *Lens Mapping*

To begin with, we choose a sufficiently large region ($\sim 3' \times 3'$) in the lens plane in which all the arcs exist. In this region we prepare regular grids. Each grid point is denoted by (x_{1i}, x_{2j}), where integers i and j are restricted in $1 \leq i, j \leq N_{\rm grid}$. In the practical calculations, we adopt $N_{\rm grid} = 8192$ throughout the paper. Given the deflection angle $\vec{\alpha}$, for all grid points we can calculate the source point $(y_1(i,j), y_2(i,j))$ which corresponds to (x_{1i}, x_{2j}) by using the lens equation.

Next we consider the source with center (y_{1c}, y_{2c}) and dimensionless radius $r_{\rm S}$ and ellipticity $e_{\rm S}$. We regard the grid point (x_{1i}, x_{2j}) is a part of lensed images if the following condition is satisfied:

$$\frac{\left[y_1(i,j)-y_{1c}\right]^2}{r_{\rm S}^2/(1-e_{\rm S})} + \frac{\left[y_2(i,j)-y_{2c}\right]^2}{r_{\rm S}^2(1-e_{\rm S})} \leq 1. \tag{18}$$

For all the grids we check this condition and obtain the pattern of lensed images. In general, multiple images can be generated by gravitational lensing. Thus we search each image grid and recognize neighboring image grids as the same image. The magnification of the image is then proportional to the number of grid points it contains.

3.3. *Detection of Arcs*

To analyze the lens properties, we calculate the magnification μ, length l, width w, orientation ϕ of the image. For the multiply lensed system, we calculate these quantities for each image.

First, the magnification is easily calculated from the number of grid points $N_{\rm image}$ which are recognized as the image; $\mu = N_{\rm image}(\Delta x)^2/\pi r_{\rm S}^2$, where Δx is the dimensionless interval of grids. This gives fairly accurate values because an image contains many grid points in our calculations; typically $N_{\rm image} \sim 600$. Next we calculate the length as follows. First we search the center of the image C as the point at which the value of the left hand side in equation (18) becomes smallest. Then we find the point A in the image which is farthest away from the center. Then we find the point B, also along the image, which is farthest away from the point A. We calculate the length of the image by $l = \overline{\rm AC} + \overline{\rm BC}$. The width is simply taken such that $\pi l w = \mu\pi r_{\rm S}^2$. We define the orientation of the image as the angle between the normal of the segment joining A and B and the segment joining the origin and the center of the image. The orientation ϕ takes the values in the range of $0^\circ \leq \phi \leq 90^\circ$.

Using the above quantities, we define the tangential and radial arcs as

$$\text{Tangential arc}: \ \frac{l}{w} \geq \epsilon_{\rm th} \ \text{ and } \ \phi \leq 40^\circ, \tag{19}$$

$$\text{Radial arc}: \ \frac{l}{w} \geq \epsilon_{\rm th} \ \text{ and } \ \phi \geq 50^\circ, \tag{20}$$

where $\epsilon_{\rm th}$ is the threshold axis ratio. The validity of this selection criterion is discussed in §5.

TABLE 1
THE CANONICAL PARAMETER SET USED IN THIS PAPER

Parameters	Values
Number of grids	8192^2
Lens mass	$10^{15}h^{-1}M_{\odot}$
Lens redshift	0.3
Source redshift	1.2
Source diameter	$0.5''$

A canonical parameter set used in this paper is summarized in Table 1. With this number of grids, a single mapped image contains typically ~ 600 grids, so it is sufficient to resolve the shape of images. We examine the shapes of the images of $50000 \sim 200000$ sources and then estimate the cross sections. We also estimate errorbars of numerically calculated cross sections simply by statistical errors.

4. NUMERICAL CALCULATION OF CROSS SECTIONS

We numerically calculate the cross sections for tangential and radial arcs using the method described in §3. First we show examples of simulated images with and without ellipticities in Figure 3. These plots clearly show that the effects of ellipticities are indeed large and cannot be neglected. Therefore, in this section, we numerically study the effects of source and lens ellipticities as well as the finite source size effect.

In Figure 4, to check simulated cross sections, we plot the lensing cross sections for tangential and radial arcs against the source redshift $z_{\rm S}$, in the case of no ellipticities. The density

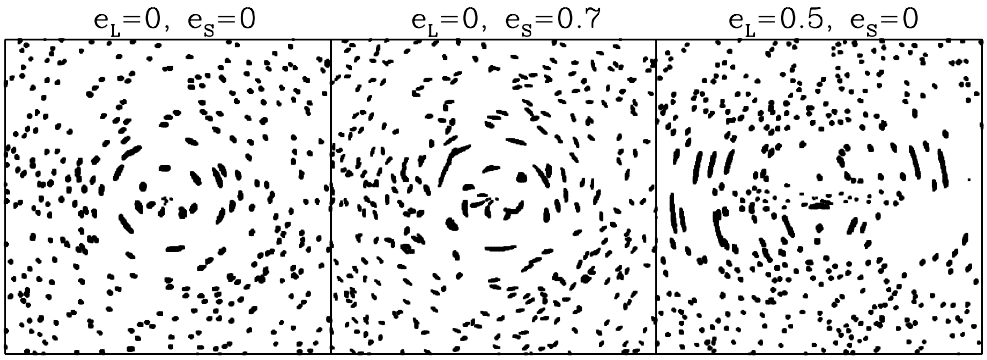

FIG. 3.— Snapshots of simulated images with and without ellipticities, produced from the same spatial distribution of source galaxies. The source ellipticity is denoted by e_S (eq. [18]) while the lens ellipticity is e_L (eqs. [16] and [17]).

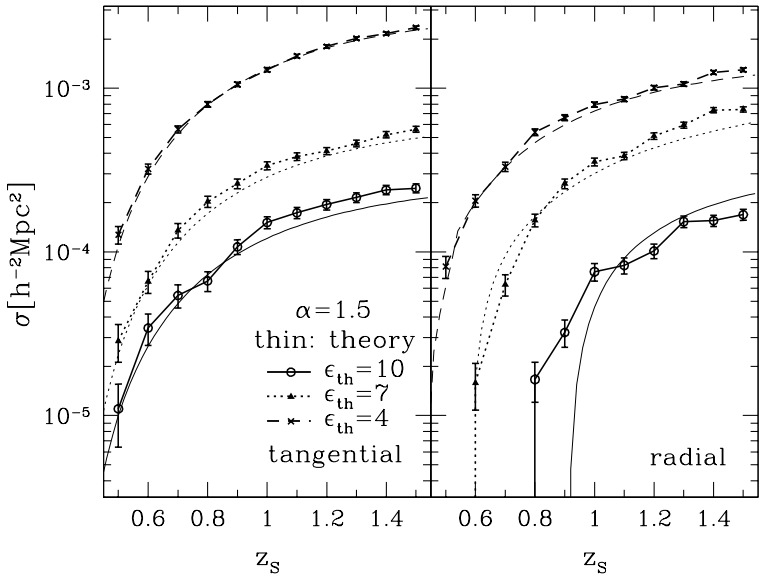

FIG. 4.— The lensing cross sections for tangential (*left panel*) and radial (*right panel*) arcs, derived from numerical simulations, against the source redshift z_S. Ellipticities are not included. The density profile is the generalized NFW profile (eq. [13]) with $\alpha = 1.5$. For the detection of arcs, three criteria of axis ratio are adopted; $\epsilon_{th} = 10$ (*solid*), 7 (*dotted*), and 4 (*dashed*). The errorbars indicate statistical errors in estimating the cross sections numerically. Thin lines are theoretical predictions which are calculated from equation (2) for tangential arcs and equation (11) for radial arcs.

profile is the generalized NFW profile (eq. [13]) with $\alpha = 1.5$. In what follows, we consider three criteria of axis ratio for the detection of arcs; $\epsilon_{th} = 10$, 7, and 4. Theoretical predictions, which are calculated from equation (2) for tangential arcs and equation (11) for radial arcs, are also plotted in thin lines. These plots make sure that the cross sections for tangential and radial arcs show good agreement between theoretical predictions and simulations.

4.1. *Finite Source Size*

In Figure 5, we show the effect of the finite source size. We also plot the theoretical prediction of cross sections for radial arcs (eq. [11]) and find that our analytic calculations show fairly good agreement with simulations. These plots clearly indicate that the source size severely affects the cross section for radial arcs. The longer arcs (larger ϵ_{th}) are more strongly affected by the source size than shorter arcs. Therefore, we need to know the source size and properly take account of the finite source size effect in calculating the number of radial arcs. On the other hand, the number of tangential arcs does not change so much within the range we examined. The typical angular diameter of sources (faint galaxies, $B \gtrsim 25$) is $\sim 1''$ (e.g., Lilly, Cowie, & Gardner 1991), and this is small compared with the cross sectional region for tangential arcs. This implies that we can estimate the lower limit of inner slope of density profile, α, from observations of radial arcs if we use the maximum cross section for radial arcs, because the density profiles with larger α usually produce the larger number of radial arcs. We also found that the size of cutoff of cross sections adopted in Oguri et al. (2001) is not so adequate, which corresponds to the width of the cross sectional region and is described by arrows in Figure 5; the cross sections begin to decrease when the source diameter ($2r_S$) is two times the cutoff width. From this figure, the cross section for radial arcs have a steep cutoff against the source size while the cross section for tangential arcs seems to decrease mildly as the source becomes larger. We conclude that the radial arcs are more sensitive to the source size effect also from this point.

4.2. *Source Ellipticity*

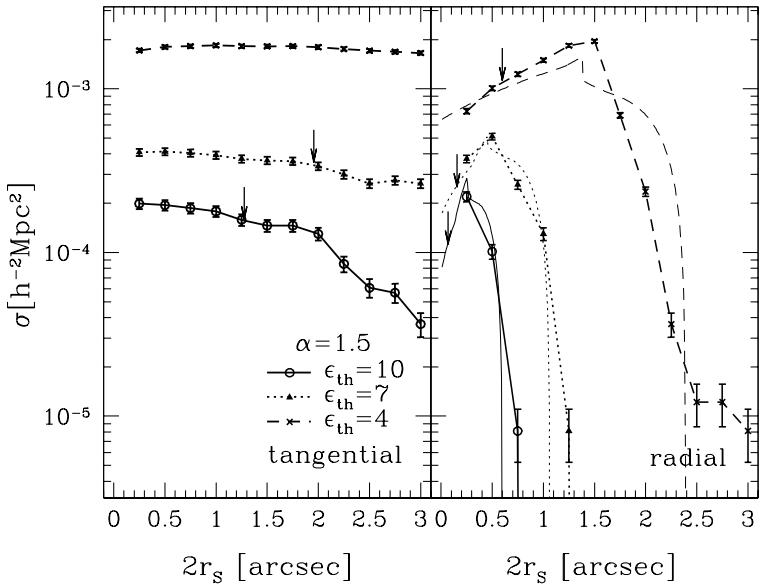

FIG. 5.— The effect of finite source size. The lensing cross sections for tangential (*left panel*) and radial (*right panel*) arcs with $\alpha = 1.5$ generalized NFW profile (eq. [13]) are plotted against the source diameter $2r_S$ in units of arcsecond. Theoretical predictions of the cross section for radial arcs (eq. [11]) are shown by thin lines. Arrows indicate the cutoff size of cross sections adopted in Oguri et al. (2001). Note that the typical angular diameter of sources (faint galaxies, $B \gtrsim 25$) is $\sim 1''$ (e.g., Lilly, Cowie, & Gardner 1991).

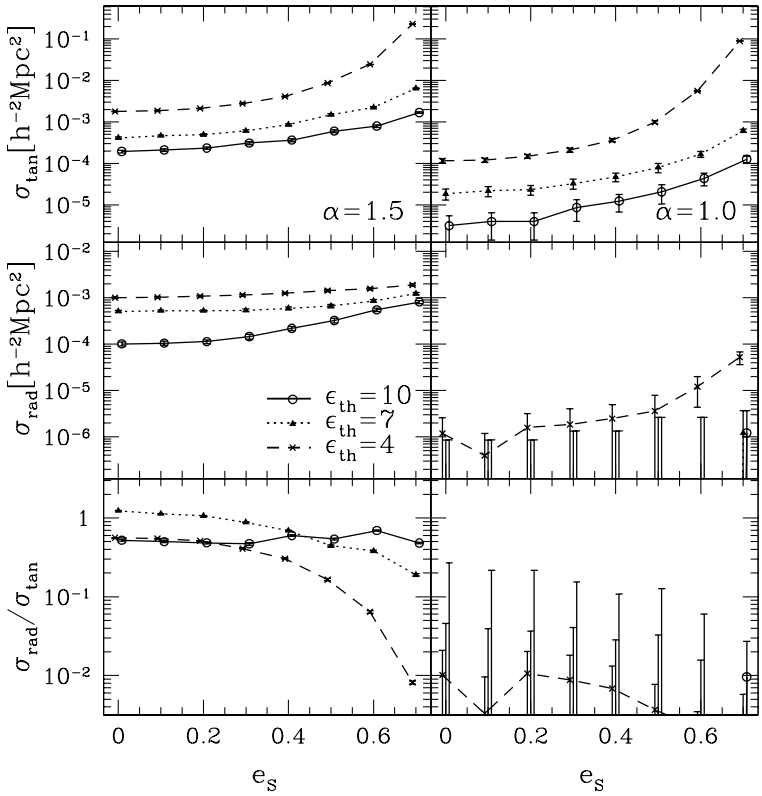

FIG. 6.— The effect of the source ellipticity. For the density profile of the lens object, we consider the generalized NFW (eq. [13]) with $\alpha = 1.5$ (*left panels*) and $\alpha = 1.0$ (*right panels*). From top to bottom, we plot the cross sections for tangential arcs, radial arcs, and the ratio of radial to tangential arcs.

Figure 6 shows the effect of the source ellipticity. As pointed out by Keeton (2001), the source ellipticity increases the number of both tangential and radial arcs, but decreases the number ratio of radial to tangential arcs. Although Keeton (2001) analytically derived the cross section including the source ellipticity assuming the infinitesimal source size and showed the above dependence, we confirmed this by the numerical simulations where sources have the finite size. Keeton (2001) only considered $\epsilon_{\rm th} = 10$ case, but we also consider $\epsilon_{\rm th} = 7$ and 4 and find that arcs with the smaller threshold values are more sensitively affected by the source ellipticities. In conclusion, except for the $\epsilon_{\rm th} = 4$ case, the number ratio of radial to tangential arcs seems not to be severely affected by source ellipticity; the difference between $\alpha = 1.5$ and $\alpha = 1.0$ is much larger than the change due to the source ellipticity.

4.3. *Lens Ellipticity*

The effect of the lens ellipticity is shown in Figure 7. As previously indicated by Bartelmann et al. (1995), lens ellipticity drastically changes the total number of arcs; more than two orders of magnitude from $e_{\rm L} = 0$ to $e_{\rm L} = 0.5$. The lens ellipticity amplifies the numbers of both tangential and radial arcs. In particular, $\alpha = 1.5$ profile and $\alpha = 1.0$ profile can produce almost the same number of tangential arcs when $e_{\rm L} = 0.5$. Nevertheless, the number ratio of radial to tangential arcs is not affected much by the lens ellipticity. Even in the case of $e_{\rm L} = 0.5$, however, the number ratio of radial to tangential arcs changes less than one order of magnitude compared with the spherical lens and is still about one order of magnitude different between $\alpha = 1.5$ and $\alpha = 1.0$. Therefore, we conclude that the number ratio remains a good indicator for halo density profile which does not so affected by the uncertainty of the lens ellipticity as to hide the difference caused by the density profile.

4.4. *Mass Dependence of Ellipticity Effects*

In the above examples, we consider the massive halo with mass $M = 1.0 \times 10^{15} h^{-1} M_\odot$ only. While this is quite typical mass of lensing clusters, it is important to check whether our qualitative results described above remain valid for less massive halos. Therefore in this subsection we see the effects of source and lens ellipticities for halos with different mass.

The results are shown in Figure 8. We plot the cross sections for three halos with different mass; $M = 1.0 \times 10^{15} h^{-1} M_\odot$, $7.5 \times 10^{14} h^{-1} M_\odot$, and $5.0 \times 10^{14} h^{-1} M_\odot$. In this plot we fix the threshold axis ratio as $\epsilon_{\rm th} = 7$ and examine only extreme cases, $e_{\rm S} = 0.7$ and $e_{\rm L} = 0.5$, as well as the case of no ellipticities. This figure clearly shows that our qualitative results are not affected at all by changing the mass of the lens object; the values of cross sections show quite similar behavior for halos with different mass. Therefore our results are generic and applicable to a wide range of the lens mass. Moreover, it seems that the number ratio of radial to tangential arcs is highly insensitive to the mass of halos, especially for the cases including ellipticities. This means that the uncertainty arising from the lens mass in determining the density profile is quite small.

5. VALIDITY OF THE SELECTION CRITERION FOR TANGENTIAL AND RADIAL ARCS

In equations (19) and (20), we discriminated tangential and radial arcs by the orientation ϕ. We regard arcs with $\phi \leq 40^\circ$ as tangential arcs and with $\phi \geq 50^\circ$ as radial arcs. There is, however, no obvious reason to adopt this selection criterion. It may be possible that tangential and radial arcs are misinterpreted with each other. Therefore, we check the validity of our selection criterion in the extreme cases we examined: $e_{\rm L} = 0.5$ and $e_{\rm S} = 0.7$. Figure 9 shows the distances of arcs from the center of the lens against the orientations of arcs defined in §3.3. This figure suggests that our selection criterion distinguishes tangential and radial arcs quite well for $e_{\rm S} = 0.7$ cases. In the $e_{\rm L} = 0.5$ cases, however, there seems to be mixing between both arcs. In particular, the case with $e_{\rm L} = 0.5$ and $\alpha = 1.0$ produces "radial" arcs which have $\phi \geq 50^\circ$ but seem to be connected with tangential arcs in the ϕ-$x_{\rm arc}$ plane. The fraction of such arcs, however, is small for longer arcs ($\epsilon_{\rm th} \gtrsim 7$). Therefore, it is safe to use our selection criterion of tangential (eq. [19]) and radial arcs (eq. [20]), especially for $\epsilon_{\rm th} \gtrsim 7$.

6. SUMMARY

We have studied several systematic effects which may change the number of tangential and radial arcs. More specifically, we have examined the effect of the finite source size, source ellipticity, and lens ellipticity.

First we derived an expression of the cross section for radial arcs (eq. [11]) taking account of the finite source size, assuming spherical lenses. We found that the cross section is enhanced by the moderate amount of the source size, while larger source size (source diameter $\gtrsim 1''$) rapidly decreases the probability of producing the radial arcs. We also derived the cross section for tangential and radial arcs numerically and confirmed that radial arcs are more sensitive to the finite source size effect than tangential arcs. It has been also found that our analytic prediction of the cross section for radial arcs shows fairly good agreement with the numerical simulations. Therefore, one can accurately predict the number of radial arcs with an arbitrary source size.

In addition to the finite source size effect, we studied effects of lens and source ellipticities. We found that both ellipticities can change the number of both tangential and radial arcs significantly; the enhancement can become as large as two orders of magnitude. The number ratio of radial to tangential arcs is, however, not so affected by ellipticities. Even in the extremely elliptical cases, the number ratio changes less than one order of magnitude on average, and still remains the difference between $\alpha = 1.5$ and $\alpha = 1$ profiles. The exception is the arcs with $\epsilon_{\rm th} = 4$. Such short arcs are more severely affected by the source ellipticity; the number ratio becomes much smaller compared with no ellipticity case. Although the these results are obtained for one specific halo with mass $M = 10^{15} h^{-1} M_\odot$, we also examined the effects of ellipticities for several halos with different mass and confirmed that our qualitative results remain valid. As a conclusion, number ratio of radial and tangential arcs with high threshold axis ratio $\epsilon_{\rm th} \gtrsim 7$ is quite robust for the uncertainties of ellipticities.

In summary, the number ratio of radial to tangential arcs which have the large axis ratio ($\gtrsim 7$) becomes good statistics which can probe the density profile of the lens object, if the source size effect is correctly taken into account. If we use the maximum cross section for radial arcs for the theoretical prediction, observations of tangential and radial arcs mainly give the lower limit of the inner slope α because the effects of ellipticities as well as the source size decrease the fraction of radial arcs. On the other hand, the total number of tangential arcs, which is also highly sensitive to the density profile of the lens object (Oguri et al. 2001), should be carefully calibrated with the ellipticities of the lens and source. Since the detailed non-

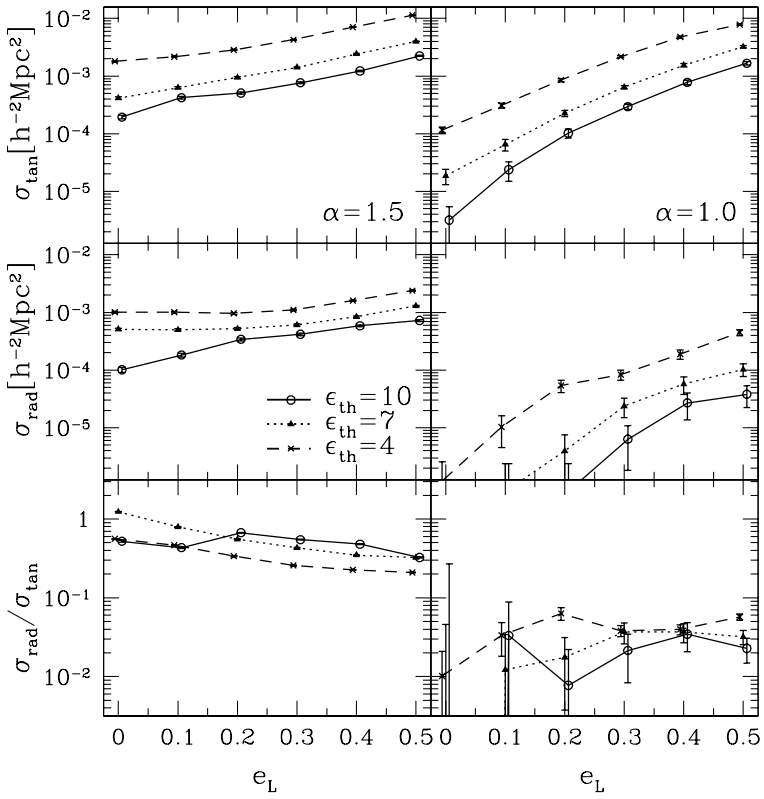

FIG. 7.— Same as Figure 6, but the plots against the lens ellipticity.

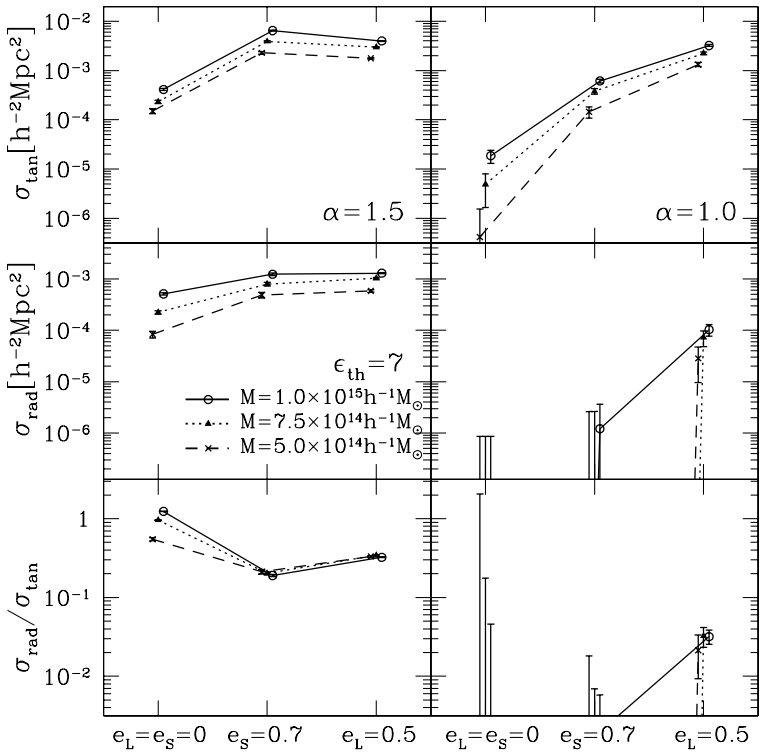

FIG. 8.— The effect of source and lens ellipticities for different lens mass. The cross sections for three halos with different mass are plotted; $M = 1.0 \times 10^{15} h^{-1} M_\odot$ (*solid*), $7.5 \times 10^{14} h^{-1} M_\odot$ (*dotted*), and $5.0 \times 10^{14} h^{-1} M_\odot$ (*dashed*). In this plot we fix the threshold axis ratio as $\epsilon_{\rm th} = 7$. For the effect of ellipticities, we examine only following three extreme cases; no ellipticities, $e_{\rm S} = 0.7$, and $e_{\rm L} = 0.5$.

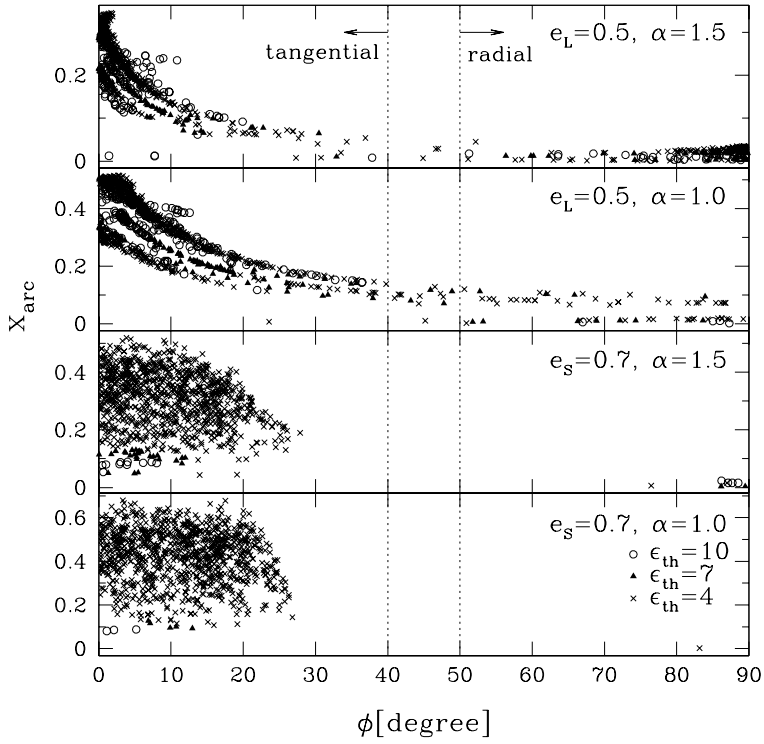

FIG. 9.— Plots for the arc positions x_{arc} against the orientations of arcs ϕ in the extreme cases we examined: e_L = 0.5 and e_S = 0.7. In each plot, we only put the points of randomly chosen 1000 arcs. Arcs with ϵ_{th} = 10, 7, and 4 are shown by open circles, filled triangles, and crosses, respectively. As shown in equations (19) and (20), we regard arcs with $\phi \leq 40°$ as tangential arcs and with $\phi \geq 50°$ as radial arcs.

spherical modeling of dark halos is now being attempted (Jing & Suto 2002), it would become an important task to take account of the effect of the lens ellipticity systematically.

Of course, there are other effects of simplifications we should consider. First, we neglect the irregularity of mass distribution in clusters. This effect, however, seems to be small enough (Flores et al. 2000; Meneghetti et al. 2000). Secondly, we neglect the effect of central cD galaxies. Radial arcs occur very close to cluster center, thus it is possible that radial arcs are hidden by the light of cD galaxies. Multicolor imaging, however, may help the identification of radial arcs because arcs have rather different color compared with those of member galaxies (Molikawa & Hattori 2001). More importantly, the gravitational potential of cD galaxies may have serious effects on arcs, especially for radial arcs (Miralda-Escudé 1995; William et al. 1999; Molikawa & Hattori 2001). Discriminating the dark halo profile from the cD galaxy profile in the central region is in general difficult because the gravitational lensing can probe only the sum of these profiles. Therefore, it may be needed to use the sample of clusters without cD galaxies to probe the density profile of dark halos.

I would like to thank Yasushi Suto and Atsushi Taruya for useful discussions and comments. I also thank an anonymous referee for helpful comments.

REFERENCES

Bartelmann, M. 1995, A&A, 299, 11
Bartelmann, M. 1996, A&A, 313, 697
Bartelmann, M., Steinmetz, M., & Weiss, A. 1995, A&A, 297, 1
Bartelmann, M., & Weiss, A. 1994, A&A, 287, 1
Bullock, J. S., Kolatt, T. S., Sigad, Y., Somerville, R. S., Kravtsov, A. V., Klypin, A. A., Primack, J. R., & Dekel, A. 2001, MNRAS, 321, 559
Flores, R. A., Maller, A. H., & Primack, J. R. 2000, ApJ, 535, 555
Golse, G., & Kneib, J. P. 2002, A&A, submitted (astro-ph/0112138)
Hattori, M., Watanabe, K., & Yamashita, K. 1997, A&A, 319, 764
Jing, Y. P., & Suto, Y. 2000, ApJ, 529, L69
Jing, Y. P., & Suto, Y. 2002, ApJ, in press (astro-ph/0202064)
Keeton, C. R. 2001, ApJ, 562, 160
Keeton, C. R., & Madau, P. 2001, ApJ, 549, L25
Lilly, S. J., Cowie, L. L., & Gardner, J. P. 1991, ApJ, 369, 79
Meneghetti, M., Bolzonella, M., Bartelmann, M., Moscardini, L., & Tormen, G. 2000, MNRAS, 314, 338
Meneghetti, M., Yoshida, N., Bartelmann, M., Moscardini, L., Springel, V., Tormen, G., & White S. D. M. 2001, MNRAS, 325, 435
Meneghetti, M., Bartelmann, M., & Moscardini, L. 2002, MNRAS, submitted (astro-ph/0201501)
Miralda-Escudé, J. 1993a, ApJ, 403, 497
Miralda-Escudé, J. 1993b, ApJ, 403, 509
Miralda-Escudé, J. 1995, ApJ, 438, 514
Molikawa, K., & Hattori, M. 2001, ApJ, 559, 544
Molikawa, K., Hattori, M., Kneib, J. P., & Yamashita, K. 1999, A&A, 351, 413
Navarro, J. F., Frenk, C. S., & White, S. D. M. 1996, ApJ, 462, 563
Navarro, J. F., Frenk, C. S., & White, S. D. M. 1997, ApJ, 490, 493
Oguri, M., Taruya, A., & Suto, Y. 2001, ApJ, 559, 572
Schneider, P., Ehlers, J., & Falco, E. E. 1992, Gravitational Lenses (New York: Springer)
Tyson, J. A., Kochanski, G. P., & Dell'Antonio I. P. 1998, ApJ, 498, L107
Williams, L. L. R., Navarro, J. F., & Bartelmann, M. 1999, ApJ, 527, 535
Wu, X.-P., & Hammer, F. 1993, MNRAS, 262, 187